Research Article

Ultra-Wideband 1–20 GHz Non-Contact FMR Test System for TMR HGA

Alongkorn Namahoot and Suramate Chalermwisutkul*
Department of Electrical and Software Systems Engineering, The Sirindhorn International Thai-German Graduate School of Engineering, King Mongkut's University of Technology North Bangkok, Bangkok, Thailand

Prayoot Akkaraekthalin
Department of Electrical and Computer Engineering, Faculty of Engineering, King Mongkut's University of Technology North Bangkok, Bangkok, Thailand

* Corresponding author. E-mail: suramate.c.ce@tggs-bangkok.org DOI: 10.14416/j.asep.2019.09.005
Received: 24 May 2019; Revised: 4 September 2019; Accepted: 9 September 2019; Published online: 30 September 2019

Abstract
The read sensor of hard disk drive abnormality at the bar level is detected by a ferromagnetic resonant analyzer (FMRA) system requiring a galvanic contact to the sensor. After the read head is assembled to the slider, a quasi-static tester is used to check the slider functionality. At this stage, the FMR information of the read sensor cannot be easily accessed since there is no suitable measurement technique available. In this research, an innovative non-contact ferromagnetic resonant (FMR) measurement for the read head sensor quality control at slider level is reported for the first time. The proposed test system is designed for detecting the FMR from 1 to 20 GHz. The FMR is interpreted from the peak of read sensor resistance over the frequency span. This new measurement technique has been applied to a model of tunneling magnetoresistance (TMR) sensor and compared with the FMRA. The FMR frequency at 5.4 GHz can be detected by the proposed measurement system with only 1 MHz difference from the value obtained from conventional FMRA. The higher effective stiffness field of the read sensor is also observed from the lower FMR resistance in the shorter stripe height head.

Keywords: Ferromagnetic resonance of TMR, Read head FMR test, FMR test for HGA, TMR sensor test

1 Introduction

The increasing demand for digital data storage for computing data and multimedia for personal devices as well as for modern cloud data center requires high capacity from magnetic recording media i.e. hard disk drives (HDD). The innovations of HDD technology such as perpendicular magnetic recording (PMR), hybrid enhanced cache (HEC), shingled magnetic recording (SMR), two dimensional magnetic recording (TDMR), heat-assisted magnetic recording (HAMR) and heated dot magnetic recording (HDMR) achieve in high aerial density larger than one terabit bit per square inch and lower that cost of the high-performance HDD [1]–[3].

The manufacturing of HDD consists of a series of assembly processes and tests. Assembling HDD consists of four main processes: wafer production, slider production, head gimbal assembly (HGA), and final hard disk drive assembly [4]. In each process, there are relevant electrical tests to assure product quality and reliability. The read-write heads on the wafer are cut into row bars for manufacturing the air bearing surface (ABS). The bar is put into a read-sensor tester called ferromagnetic resonance analyzer (FMRA). The FMRA measures the thermal magnetization fluctuation

Please cite this article as: A. Namahoot, S. Chalermwisutkul, and P. Akkaraekthalin, "Ultra-wideband 1–20 GHz non-contact FMR test system for TMR HGA," *Applied Science and Engineering Progress*, vol. 14, no. 2, pp. 284–294, Apr.–Jun. 2021, doi: 10.14416/j.asep.2019.09.005.

noise spectrum in the frequency range from 0.3 to 10 GHz transverse to a cross-track magnetic field while a longitudinal external magnetic field is aligned in parallel with the magnetization of the free layer of the sensor. The noise spectrum measured by the FMRA [5].

The FMRA reveals the effective stiffness field of the free layer, alignment deviation of effective free layer magnetization from the cross-track direction and the symmetry of read head from spectral shift due to the transverse magnetic field. The FMRA uses the measurement principle based on the broadband noise spectra measurement [6]–[9]. After testing the sensor bar, the bar is singulated into the sliders. The slider is assembled to an arm forming a head gimbal assembly (HGA). The finished HGA is then tested by a commonly used electrical test called quasi-static test (QST) to identify the head problems in the early stages of the manufacturing process [10]. The QST measurement is based on the combination of magnetoresistance (MR) measurement of the read head and the noise under uniform external magnetic fields normal to the ABS. The transfer curve of QST can be used to screen the normal sensor with the linearly symmetrical response of amplitude from the defective sensor with nonlinear, strong amplitude asymmetry, soft- and hard-kinks, hysteretic and low amplitude. The transfer curve reflects the macroscopic magnetic state of the sensing layer which is the free layer [11]. After the test, the tail of the HGA is cut and assembled with final HDD. The test time of QST at HGA level is very fast and the cost of this test is very low so that it can be efficiently multiplied and installed in the production lines. Since the test case of QST is limited to the resistance to magnetic field (R-H) curve, there is no information of frequency spectra like in the FMRA at row bar level. If there could be a FMR tester that can test the read head at the HGA level, the advantage would be the observation of abnormalities, instabilities, and degradation of the sensor after HGA assemblies which cannot be detected by QST. The direct FMRA for HGA requires an electrical contact which is not appropriate since the measurement includes the effect of traces gimbal, flexure, flexure tail, and suspension.

The read head type used in this study is the tunneling magnetoresistance (TMR) sensor with current-perpendicular-to-plane (CPP) geometry. The simplified structure of the TMR read sensor is shown in Figure 1 [12]. The TMR sensor consists of two ferromagnetic

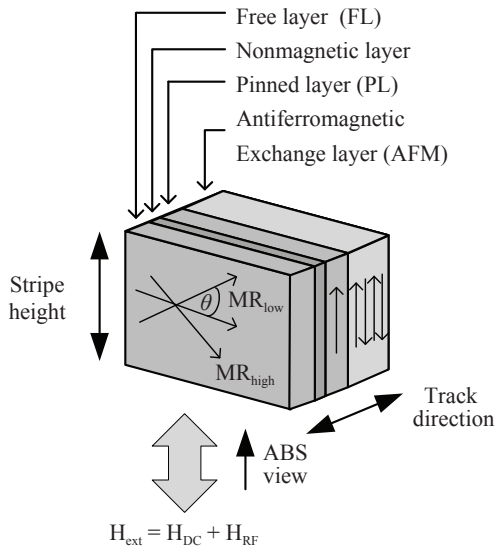

Figure 1: TMR read head sensor (reproduced from [12]).

layers: free layer (FL) and pinned layer (PL) sandwiched on a non-magnetic insulator [12], [13]. The magnetic orientation of the pinned layer is fixed by an antiferromagnetic exchange layer (AFM) also referred to as pinning layer. The magnetic orientation of the free layer is along the direction of external magnetic field from the platter.

When the magnetic orientation of the free layer is in parallel with the pinned layer's magnetic field, the MR is minimum (positive angle θ), and the current can flow through the insulator. On the other hand, when the field from free layer is anti-parallel to the pinned layer's magnetic field (negative angle θ), the magnetoresistance is maximum and impedes the current flow through the barrier. The MR is determined by the voltage across the read sensor while a constant current source is biased to the head.

This paper proposes a new FMR test method for HGA based on the application of both DC magnetic field (HDC) and non-contacted RF magnetic field (HRF) to the HGA. The frequency absorption of magnetic materials, especially FL in the read head on HGA, is translated into the resistance change of the sensor and regarded as the ferromagnetic resonance of magnetic material of FL. The frequency test range is also extended from 10 to 20 GHz, higher than a conventional FMRA.

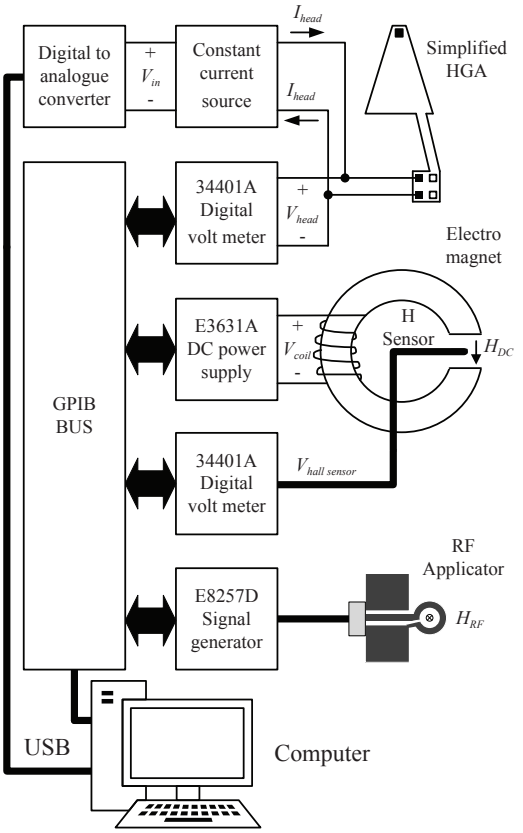

Figure 2: Proposed FMR tester block diagram.

2 Test System Design

The test system in Figure 2 consists of three subsystems: a current-bias circuit for read head biasing, a DC electromagnet for HDC generation and a RF applicator for HRF generation. The HGA is put into the middle of DC magnet and the sensor ABS is placed on the top of the RF applicator center loop as shown in Figure 3. The distance between RF applicator and ABS is 0.5 mm. The HDC direction in this test is in the same direction as in QST and with this configuration, both HDC and HRF are in the direction parallel to PL and normal to the ABS as shown in Figure 1.

2.1 *Constant current bias for the read head*

An adjustable constant current circuit uses a precision

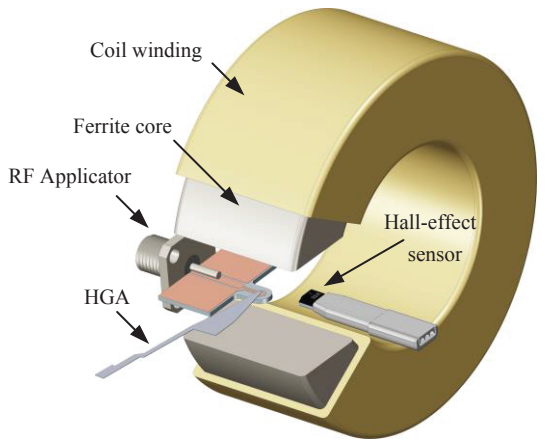

Figure 3: Simplified layout of HGA test hardware.

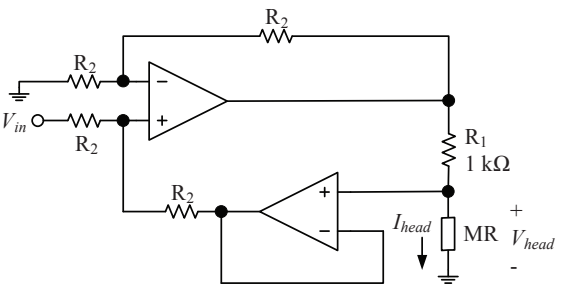

Figure 4: Precision constant current circuit.

voltage-controlled current source as shown in Figure 4 [14]. The circuit consists of a differential amplifier and a buffer circuit. The constant current flow through the read head sensor (I_{head}) can be calculated by the ratio of the input bias voltage (V_{in}) to the biased resistor (R_1) as in Equation (1).

$$I_{head}[\mathrm{A}] = \frac{V_{in}[\mathrm{V}]}{\mathrm{R}_1[\Omega]} \tag{1}$$

The read head bias current is set to 100 μA to avoid sensor damage. R_1 is chosen to be 1000 Ω and the corresponding input bias voltage 100 mV is required. The change of read head magnetoresistance from the influence of the external DC and RF magnetic field can be monitored from the voltage across the read head (V_{head}) and calculated by Equation (2).

$$\mathrm{MR}[\Omega] = \frac{V_{head}[\mathrm{V}]}{I_{head}[\mathrm{A}]} \tag{2}$$

Figure 5: The ferrite core before the cut (left) and finished DC electromagnet coil (unit: cm).

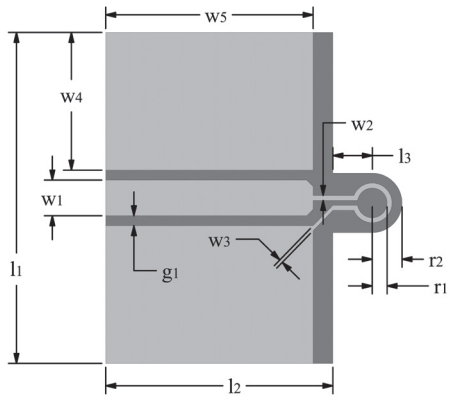

Figure 6: Geometry of the 1-20 GHz RF applicator.

2.2 *DC electromagnet*

The electromagnet is used for generating an external DC magnetic field. The field is applied to the HGA. A toroidal ferrite core with inner diameter of 38 mm and outer diameter of 64 mm is chosen instead of using an iron core to avoid residue magnetic field when the coil current is off. The initial permeability of the core (μ_i) is 10,000. An air gap of 20 mm on the core is cut by waterjet to form the C-shape. The final core is wound with an enameled copper wire number SWG32 for 600 turns as shown in Figure 5. With this coil configuration, the maximum magnetic field of +300 Oe can be achieved with high current DC power supply. The generated DC magnetic field strength is governed by a Hall effect sensor. The sensor is mounted within the air gap of the magnetic core and has an output sensitivity of 1.34 mV per Oersted. The field is calibrated against the Gauss meter for correctness.

2.3 *RF applicator*

An RF applicator is designed for a broadband magnetic near-field source for the frequency from 1 to 20 GHz. A simple single loop coil structure depicted in Figure 6 is chosen since the volume of generated field is small and mostly oriented in the normal direction to the substrate according to Ampère's circuital law [15], [16]. This field can be greatly concentrated on the read head sensor under test. The circuit consists of a 50-Ω coplanar waveguide (CPW) on a 1.0 mm FR-4 substrate and a circular loop for returning the signal to ground. The middle conductor width and the gap between signal and ground are calculated by a quasi-TEM analytical formula as described in [17] and yield a value of w_1 = 1.8 mm and g_1 = 0.2 mm, respectively. The ending of the circular trace has an inner radius r_1 = 0.75 mm and the track width w_2 = 0.25 mm. The circuit geometry is tuned to maximize the magnetic field strength in z-direction normal to the loop. The final applicator geometrical parameters are listed in Table 1. To demonstrate the measurement of the actual field generated from the applicator, the in-house development shielded magnetic near-field probe is used to measure the field [18]. The measurement configuration is shown in Figure 7. The magnetic probe is located at 0.5 mm above the applicator coil center to avoid loading effect from the probe body. A swept-continuous wave generator is connected to the applicator. The amplitude is set to 10 dBm and the frequency is swept from 1 to 20 GHz.

Table 1: Geometrical parameters of the proposed RF magnetic field applicator

Parameter	Value (mm)	Parameter	Value (mm)
w_1	1.80	l_1	17.00
w_2	0.25	l_2	11.50
w_3	0.17	l_3	2.00
w_4	6.95	r_1	0.75
w_5	10.50	r_2	1.50
g_1	0.5		

The output of the magnetic probe is connected to the spectrum analyzer and the magnitude of the output signal is measured. The actual magnetic field generated by the coil at its center can be calculated from the output power of the magnetic probe and the probe factor (PF). The probe factor is calculated from the ratio of the calculated magnetic field to the induced

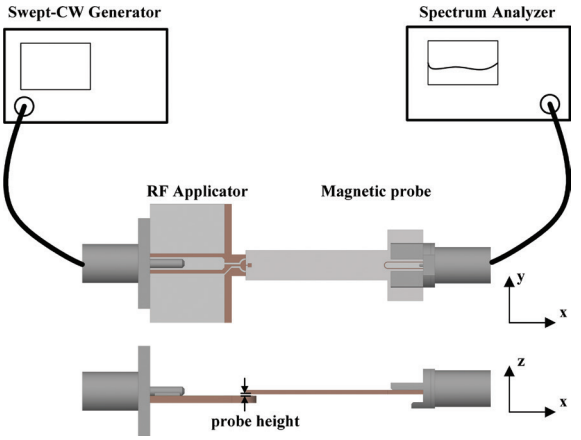

Figure 7: The measurement of the magnetic field from RF applicator.

voltage of the probe as in Equation (3) [19].

$$PF\left[\mathrm{dBS/m}\right] = 20 \cdot \log\left(\frac{H_{theory}\left[\mathrm{A/m}\right]}{V_{ref}\left[\mathrm{V}\right]}\right) \quad (3)$$

Where H_{theory} is the theoretical magnetic field generated by a reference microstrip line and V_{ref} is the measured voltage of the magnetic probe. To make it more convenient, the probe factor can be calculated from the output power of the probe measuring the magnetic field from the reference microstrip line (P_{ref}). Therefore, the probe factor can also be expressed as:

$$PF\left[\mathrm{dBS/m}\right] = H_{theory}\left[\mathrm{dBA/m}\right] - P_{ref}\left[\mathrm{dBm}\right] + 13 \quad (4)$$

The actual magnetic field (H_{actual}) generated from the device under test (DUT) at the same probe height can be simply determined from the probe factor from Equation (4) and the output power of the magnetic probe readout from spectrum analyzer (P_{meas}) as follows [Equation (5)]:

$$H_{actual}\left[\mathrm{dBA/m}\right] = PF\left[\mathrm{dBS/m}\right] + P_{meas}\left[\mathrm{dBm}\right] - 13 \quad (5)$$

PF of the proposed magnetic probe is shown in Figure 8. Since the RF cables and the spectrum analyzer setting (frequency span, resolution bandwidth, and attenuation level) are identical to the measurement set-up when performing probe factor measurement, there is no need to de-embed the RF cable and RF connector

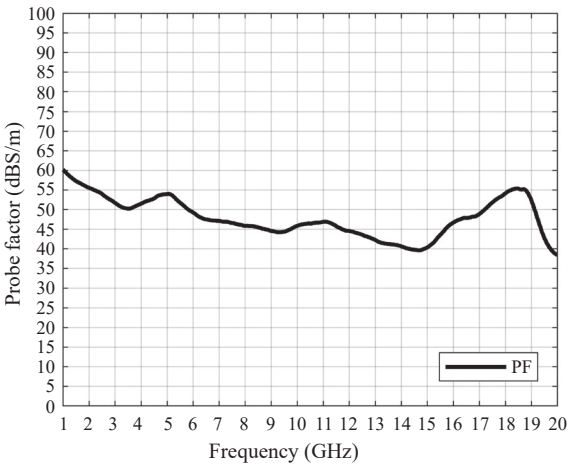

Figure 8: Probe factor (PF) of the proposed magnetic probe.

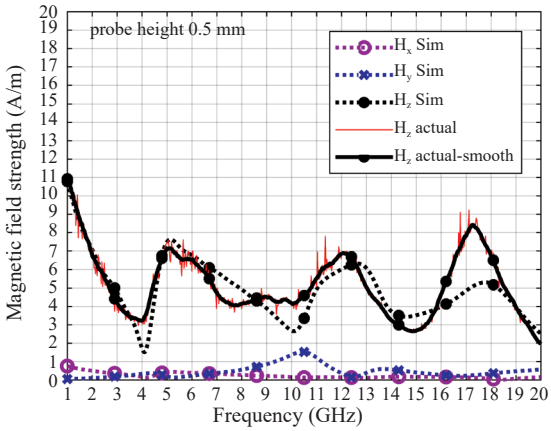

Figure 9: Actual magnetic field and simulated magnetic field from the applicator at 0.5 mm.

losses from the actual magnetic field calculation. The actual magnetic field and simulated magnetic field are compared as shown in Figure 9. The simulated fields are calculated under the unloaded condition (no magnetic probe) and the result shows that the field component in z-direction is the largest. The actual field shows very good agreement with the calculation except from the values in the frequency range between 16–18 GHz. This excessive build-up voltage at the probe might be caused by the leak of the electric field to the probe. Nevertheless, it is proven that the proposed applicator can be used for generating the RF magnetic field with a field strength higher than 2 A/m for the entire frequency band with the RF input power of 10 dBm.

3 Test Procedure

An automated GPIB software is developed to control the test parameters and acquire the read head resistance. To start the test, the read head is biased with a current of 100 μA. The RF power from 0 to 10 dBm and the frequency from 1 to 20 GHz are applied to the RF applicator for HRF generation. The DC magnetic is initially set to zero Oersted and the measurement software starts to collect the read head resistance.

The resistance is calculated from the readback voltage with Equation (2) until the end of the cycle. To reduce the data variation, the software collects 100 measurements for each setting and use their median to represent a single data. The measurement is then repeated for HDC setting to 100, 200, and 300 Oe.

The FMR frequency of the read head represents the frequency at which a strong change of resistance is caused by RF energy absorption. The RF energy can be absorbed by various components including the read head magnetic material, sensor shield, HGA arm, and surrounding materials. The RF power is increased from 0 to 10 dBm and the resistance changes can be clearly observed with the RF power of 10 dBm. At 0 dBm, there is no level change of the resistance compared to the case when the RF power is turned off.

To isolate the sensor shield absorption, high external DC magnetic field is used to saturate the shield. Since the maximum HDC of the proposed system is 300 Oe, this value is used. To reduce the data variation, the difference of MR in case of high RF field and MR in case of low RF field is calculated with Equation (6). This quantity represents the MR change caused by the sensor's magnetic material and other materials under the shield saturation condition.

The MR change due to HRF absorption at zero DC magnetic field is determined by Equation (7). This resistance change is caused by the read head's magnetic material and other materials under the unsaturated shield condition. To extract the FMR frequency, subtraction of the resistance difference with unsaturated shield from the resistance difference with saturated shield yields the resistance change caused only by the sensor's magnetic material as represented in Equation (8).

$$\Delta MR_{300\ Oe} = MR_{300\ Oe,\ 10\ dBm} - MR_{300\ Oe,\ 0\ dBm} \quad (6)$$

$$\Delta MR_{0\ Oe} = MR_{0\ Oe,\ 10\ dBm} - MR_{0\ Oe,\ 0\ dBm} \quad (7)$$

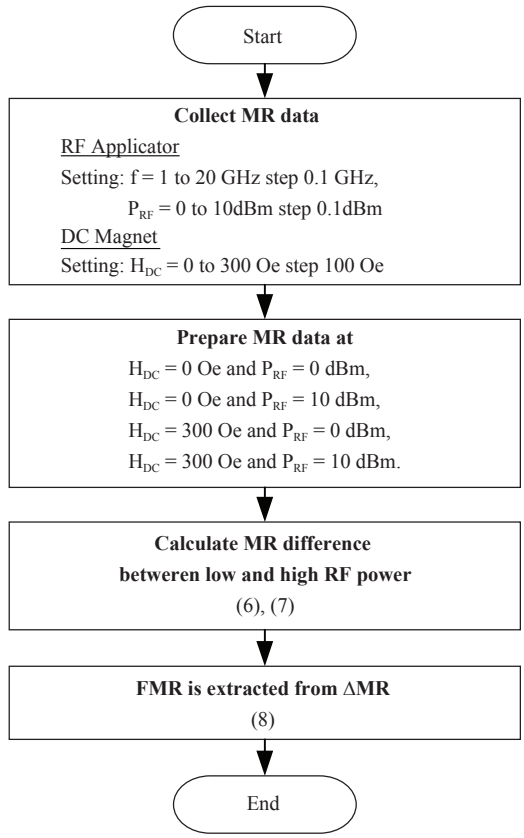

Figure 10: HGA FMR test flowchart.

$$\Delta MR = \Delta MR_{300\ Oe} - \Delta MR_{0\ Oe} \quad (8)$$

4 Results and Discussion

A HGA model is selected for testing with the proposed test system. Four HGA samples with nominal MR of 350, 450, 550, and 750 Ω are used in this study. The sensor resistance is different because of the tolerance of sensor stripe height from the sensor lapping process. The lower the stripe height, the higher is the resistance (Figure 10).

4.1 *350 Ω read head*

The measurement results of 350 Ω head are shown in Figures 11–13. Figure 11 presents the result from the change of resistance as a function of frequency with RF power of 10 dBm and with four different DC magnetic field strengths. There are multiple

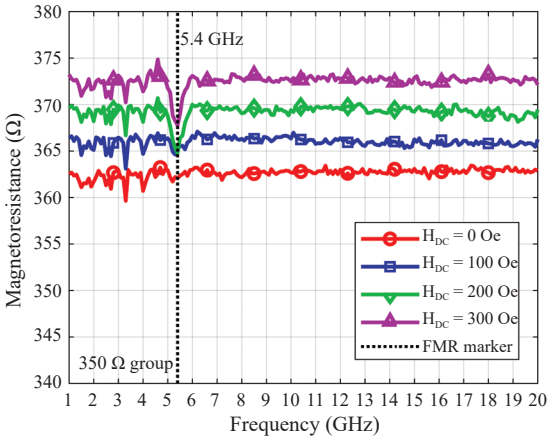

Figure 11: FMR test of 350 Ω read head with P_{RF} = 10 dBm and varied DC magnetic field.

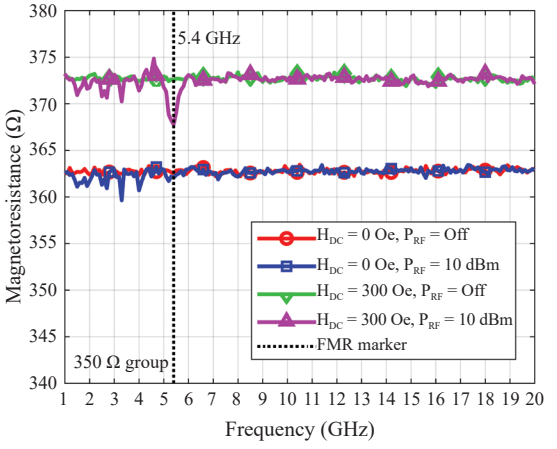

Figure 12: FMR test of 350 Ω read head with P_{RF} and DC magnetic field turned on or off.

frequency absorption points which can be observed from the MR minima especially from 1 to 6 GHz. In this case, the RF energy is absorbed by the entire HGA and also by the test fixture. The strong MR decrease caused by RF absorption with high DC magnetic field which saturates the shield is observed at 5.4 GHz. It is also shown in Figure 12 that when the RF power is turned off, there is no energy absorption at 5.4 GHz. To extract the FMR frequency due to the absorption in the read head only and not in other structures, the difference of the case with and without the DC magnetic field according to Equation (8) is shown in Figure 13. Except for the absorption at 5.4 GHz, no significant MR change

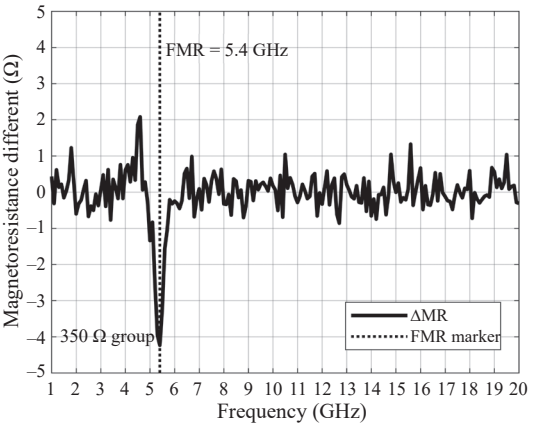

Figure 13: FMR of 350 Ω read head.

is observed at other frequencies. Thus, the FMR frequency can be determined with the proposed test method at 5.4 GHz.

4.2 *450 Ω read head*

The measurement of 450 Ω head is shown in Figures 14–16. In contrast to the case with 350 Ω sample, MR value of the 450 Ω head at the resonance is higher than in the non-resonance case as shown in Figure 14. The resistance of the resonance is decreased as the DC magnetic field is increased which is the same trend as that of 350 Ω sample. The frequency absorption caused by the material is again confirmed with high RF power of 10 dBm whereas no absorption is observed with no RF power as shown in Figure 15. The resistance difference calculation from Equation (8) confirms that the FMR frequency of 450 Ω sample is 5.4 GHz as shown in Figure 16.

4.3 *550 Ω read head*

For the 550 Ω read head, the resonance resistance at 5.4 GHz is lower than the non-resonance case as the DC magnetic field is increased to 300 Oe. Without the DC magnetic field, the resonance resistance at 5.4 GHz is higher than the non-resonance case (see Figure 17). When the RF power is turned off, the resonance and other frequency absorption vanish as presented in Figure 18. The resistance difference calculated from Equation (8) is shown in Figure 19 and confirms the FMR frequency at 5.4 GHz.

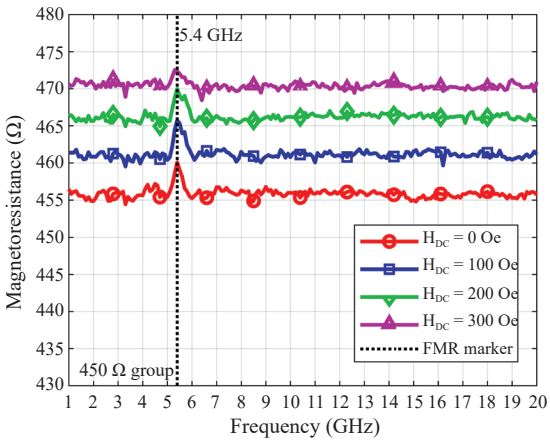

Figure 14: FMR test of 450 Ω read head with P_{RF} = 10 dBm and varied DC magnetic field.

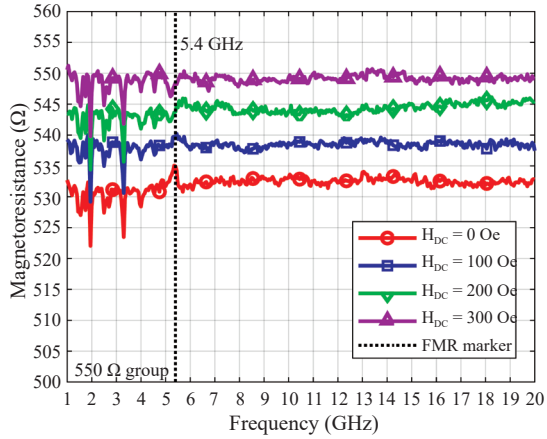

Figure 17: FMR test of 550 Ω read head with P_{RF} = 10 dBm and varied DC magnetic field.

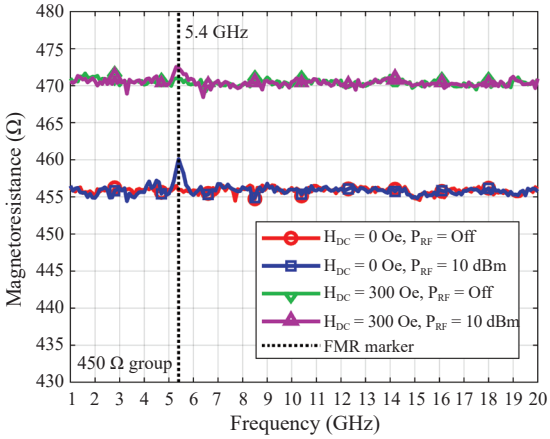

Figure 15: FMR test of 450 Ω read head with P_{RF} and DC magnetic field turned on or off.

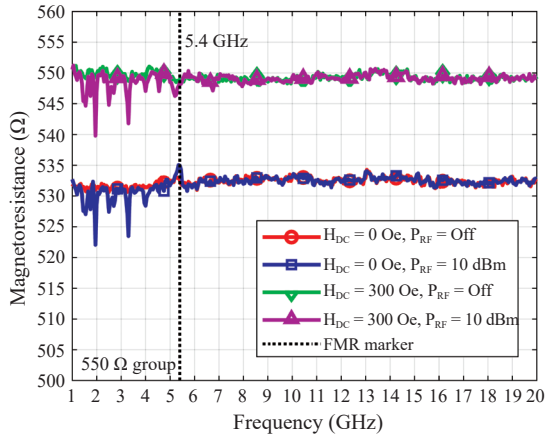

Figure 18: FMR test of 550 Ω read head with P_{RF} and DC magnetic field turned on or off.

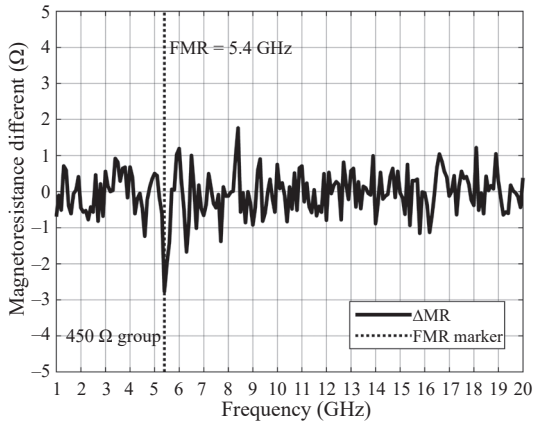

Figure 16: FMR of 450 Ω read head.

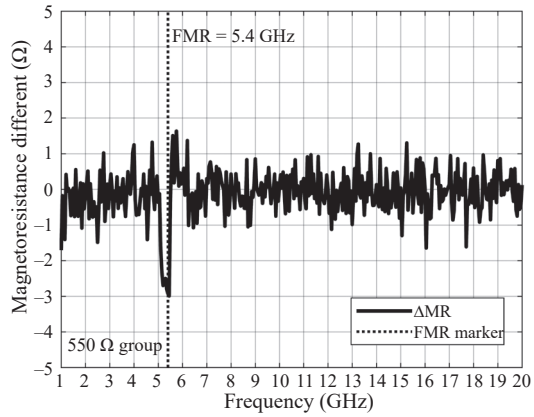

Figure 19: FMR of 550 Ω read head.

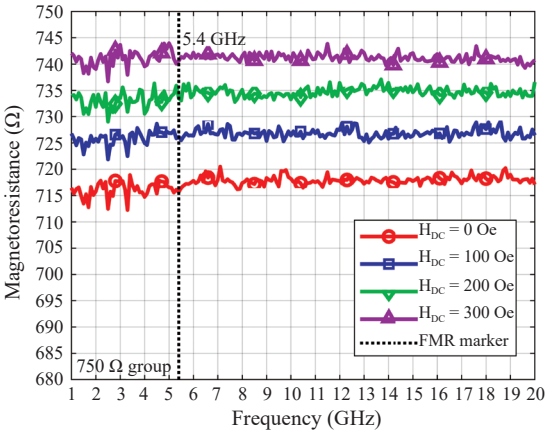

Figure 20: FMR test of 750 Ω read head with P_{RF} = 10 dBm and varied DC magnetic field.

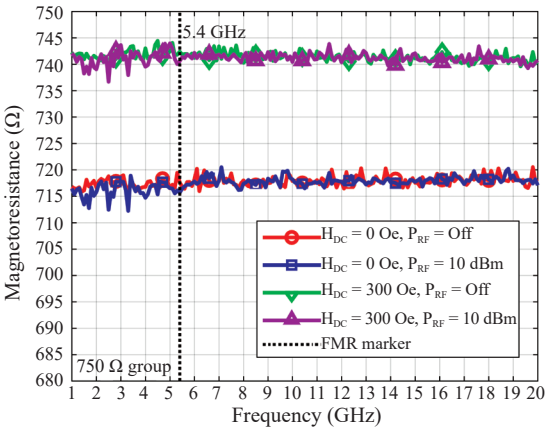

Figure 21: FMR test of 750 Ω read head with P_{RF} and DC magnetic field turned on or off.

4.4 *750 Ω read head*

Figures 20 and 21 represent the small change of resistance of 750 Ω read head. It is difficult to see the resonance at 5.4 GHz. Using Equation (8) with the data plotted in Figure 22, it cannot distinguish the FMR frequency of this sample in contrast to the case with low resistance samples.

From the test results of four different samples, all read heads response to both DC and RF magnetic fields. When the applied HDC has changed from 0 to 300 Oe, the resistance of 350, 450, 550, and 750 Ω samples are increased about 10, 15, 20, and 22 Ω, respectively. Those uptrends of resistance change

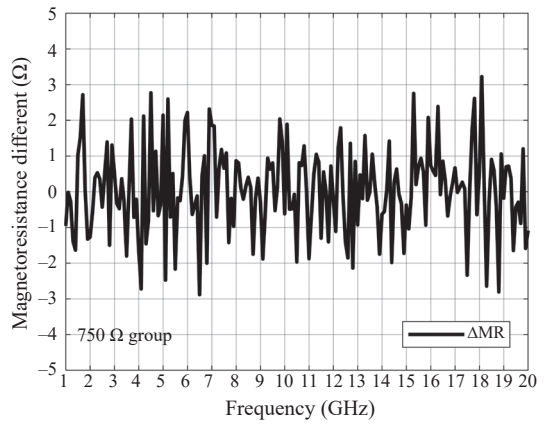

Figure 22: Resistance difference of 750 Ω read head.

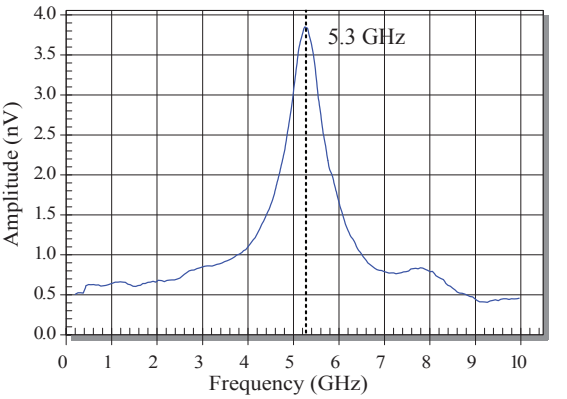

Figure 23: Noise spectra of a sensor on the bar from FMRA with zero DC magnetic field.

inherit from their stripe height. The lower the stripe height the higher the resistance and so the higher is the resistance change.

For the HRF application to the test samples, it can be found that the FMR frequency is 5.4 GHz with no further resonance observed at higher frequencies. To validate the FMR frequency measured from the proposed method, the same slider model is tested with FMRA and zero DC magnetic field, the FMR frequency is at 5.3 GHz as shown in Figure 23.

The good agreement between the proposed FMR test method and conventional FMRA is confirmed. The small difference could be caused by different measurement setup and resolution. The FMRA acquires noise level of the slider in the time domain and converts this noise signal with fast

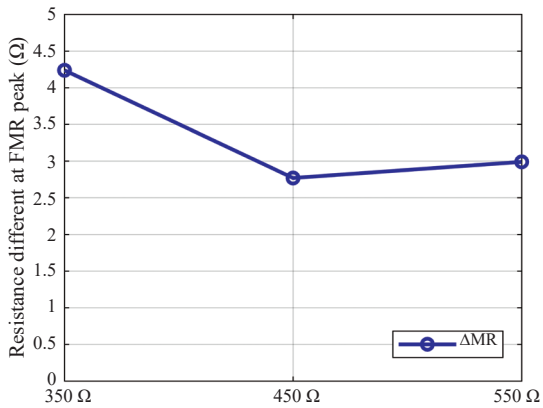

Figure 24: The change of FMR peak level on different stripe height.

Fourier transform (FFT) to the frequency domain while the proposed technique uses large-signal measurement directly in the frequency domain with external DC field and RF field in the cross direction to the free layer.

With the FMRA technique, the previous studies showed that shorter stripe height provides a higher effective stiffness field of the free layer [20]. The stiffness field is used for sensor characterization and to calculate sensor saturation magnetization. The high stiffness field is associated with an increase of FMR frequency. These sliders had similar or lower FMR peaks compared with normal head [5]. However, in the proposed test system, the lower in FMR peak could be analogous to the smaller level of MR change from zero HRF and non-zero HRF for the higher resistance group which has shorter stripe height as shown in Figure 24.

5 Conclusions

In this paper, a novel ultra-wideband 1 to 20 GHz contactless FMR tester for hard disk drive slider is proposed. The new test method utilized the application of an external DC magnetic field and an external RF magnetic field. A model of TMR read head has been tested and compared with the existing FMRA test. The FMR frequency from the proposed system is in a very good agreement with the FMR frequency from the FMRA. The proposed test method is suitable not only for finding FMR frequency for the read head sensor but also for detecting the frequency absorption from a new generation of read head with microwave-assisted magnetic recording technology. The limitation of this method is that it cannot be used to detect the FMR asymmetry, low peak and double peak since the test with very fine frequency step is time-consuming and the data interpretation is very difficult if the peak is not dominant.

To improve the test system, the use of higher power DC magnet can increase the external DC magnetic field to more than 300 Oe. It would help to saturate the shield more and the shifting of FMR frequency to the higher frequency at the high field should be observed. Also, the RF power from the applicator can be increased by using 1–20 GHz amplifier or by using alternative RF applicator design for higher RF magnetic field generation. If the RF power is higher, the FMR frequency at the short stripe height could be easier to observe.

Acknowledgments

This work has been supported by the Research and Researchers for Industries (RRi) Ph.D. Scholarship awarded by the Thailand Research Fund with the contract number PHD57I0033 and the Thailand Research Fund under the TRF Senior Research Scholar Program with the contract number RTA6080008.

References

[1] R. Mark. (2017, Dec.). Tech Talk on HDD Areal Density. Seagate Technology PLC. California, US [Online]. Available: https://www.seagate.com/www-content/ investors/_shared/docs/tech-talk-mark-re-20150825.pdf

[2] Y. Chen, D. Song, J. Qiu, P. Kolbo, L. A Wang, Q. He, M. Covington, S. W. Stokes, V. V. Sapozhnikov, D. V. Dimitrov, K. Gao, and B. M. Miller, "2 Terabit per square inch reader design outlook," *IEEE Transactions on Magnetics*, vol. 46, no. 3, pp. 697–701, 2010.

[3] M. Takagishi, K. Yamada, H. Iwasaki, H. N. Fuke, and S. Hashimoto, "Magnetoresistance ratio and resistance area design of CPP-MR film for 2–5 Tb/in^2 read sensors," *IEEE Transactions on Magnetics*, vol. 46, no. 6, pp. 2086–2089, 2010.

[4] V. Lerswanichkul and N. Rojanarowan, "Quality-based sampling test design for head gimbal

assembly," *IOSR Journal of Engineering (IOSRJEN)*, vol. 3, no. 9, pp. 57–64, 2013.

[5] A. Taratorin, "Measurement of effective free layer magnetization orientation of TMR sensors," *IEEE Transactions on Magnetics*, vol. 45, no. 10, pp. 3449–3452, 2009.

[6] K. B. Klaassen, X. Z. Xing, and J. C. L. van Peppen, "Broad-band noise spectroscopy of giant magnetoresistive read heads," *IEEE Transactions on Magnetics*, vol. 41, no. 7, pp. 2307–2317, 2005.

[7] A. V. Nazarov, H. S. Cho, J. Nowak, S. Stokes, and N. Tabat, "Tunable ferromagnetic resonance peak in tunneling magnetoresistive sensor structures," *Applied Physics Letters*, vol. 81, no. 24, pp. 4559–4561, 2002.

[8] R. J. M. van de Veerdonk and P. J. L. Beliën, "1/f noise in anisotropic and giant magnetoresistive elements," *Journal of Applied Physics*, vol. 82, no. 12, pp. 6152–6164, 1997.

[9] J. C. Jury, K. B. Klaassen, J. C. L. van Peppen, and S. X. Wang, "Measurement and analysis of noise sources in giant magnetoresistive sensors up to 6 GHz," *IEEE Transactions on Magnetics*, vol. 38, no. 5, pp. 3545–3555, 2002.

[10] Z. Jun and M. Loera, "Amplitude and asymmetry correlation study between quasistatic and dynamic electrical testing of MR sensors," *IEEE Transactions on Magnetics*, vol. 34, no. 4, pp. 1525–1527, 1998.

[11] L. Baril, B. Higgins, and A. Wallash, "Effects of ESD transients on noise in tunneling recording heads," *Journal of Electrostatics*, pp. 147–150, 2006.

[12] J. R. Childress and R. E. Fontana, "Magnetic recording read head sensor technology," *Comptes Rendus Physique*, vol. 6, no. 9, pp. 997–1012, 2005.

[13] S. Mao, Y. Chen, F. Liu, X. Chen, B. Xu, P. Lu, M. Patwari, Haiwen Xi, Clif Chang, B. Miller, D. Menard, B. Pant, J. Loven, K. Duxstad, S. Li, Z. Zhang, A. Johnston, R. Lamberton, M. Gubbins, T. McLaughlin, J. Gadbois, J. Ding, B. Cross, S. Xue, and P. Ryan, "Commercial TMR heads for hard disk drives: Characterization and extendibility at 300 gbit2," *IEEE Transactions on Magnetics*, vol. 42, no. 2, pp. 97–102, 2006.

[14] N. Zhao, R. Malik, and W. Liao, "Difference amplifier forms heart of precision current source," *Analog Dialogue*, vol. 43 no. 3, pp. 22–24, 2009.

[15] G. Yingjie and I. Wolff, "A new miniature magnetic field probe for measuring three-dimensional fields in planar high-frequency circuits," *IEEE Transactions on Microwave Theory and Techniques*, vol. 44, no. 6, pp. 911–918, 1996.

[16] K. Jung-Min, K. Woo-Tae, and Y. Jong-Gwan, "Resonance-suppressed magnetic field probe for EM field-mapping system," *IEEE Transactions on Microwave Theory and Techniques*, vol. 53, no. 9, pp. 2693–2699, 2005.

[17] G. Ghione and C. Naldi, "Analytical formulas for coplanar lines in hybrid and monolithic MICs," *Electronics Letters*, vol. 20, no. 4, pp. 179–181, 1984.

[18] A. Namahoot, P. Akkaraekthalin, and S. Chalermwisutkul, "Design of a low-cost 1-20 GHz magnetic near-field probe with FR-4 printed circuit board," *International Journal of RF and Microwave Computer-Aided Engineering*, to be published. doi: 10.1002/mmce.21958.

[19] D. Baudry, C. Arcambal, A. J.-O. Louis, B. Mazari, and P. Eudeline, "Applications of the near-field techniques in EMC investigations," *IEEE Transactions on Electromagnetic Compatibility*, vol. 49, no. 3, pp. 485–493, 2007.

[20] P. Weawhongse, C. Sa-Ngiamsak, W. Pijitrojana, and K. Vichienchom, "free layer characterization of TMR head with multi-stripe height by using ferro magnetic resonance analyzer (FMRA)," *Applied Mechanics and Materials*, vol. 781, pp. 195–198, 2015.